Supplementary Information

Motion Image Feature Extraction through Voltage Modulated Memory Dynamics in IGZO Thin-Film Transistor

*Yu-Chieh Chen,[a] Jyu-Teng Lin,[a] Kuan-Ting Chen,[a] Chun-Tao Chen [a] and Jen-Sue Chen [*a,b]*

[a] Department of Materials Science and Engineering, National Cheng Kung University, Tainan 70101, Taiwan

[b] Academy of Innovative Semiconductor and Sustainable Manufacturing, National Cheng Kung University, Tainan 70101, Taiwan

**E-mail: jenschen@ncku.edu.tw*

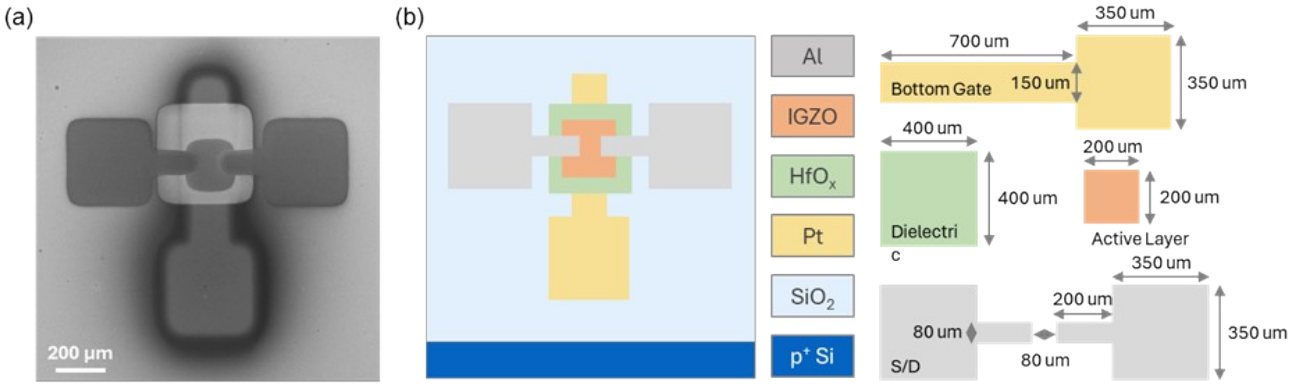

Figure S1. (a) Scanning electron microscopy (SEM) image of the fabricated IGZO TFT, illustrating the device morphology. (b) Feature size information of the IGZO TFT, providing a detailed view of the structural dimensions.

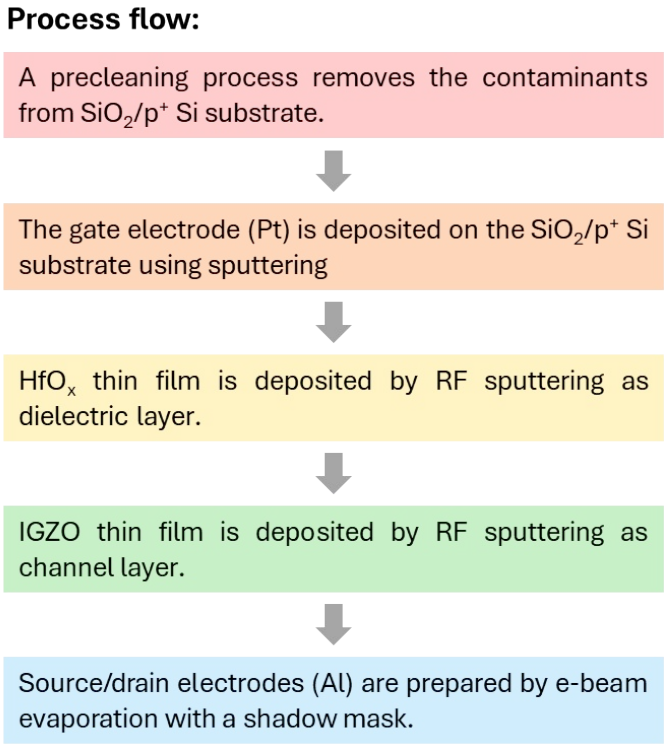

Figure S2. Process flow for the fabrication of the IGZO transistor. The process begins with substrate cleaning to remove contaminants from the SiO_2/p^+ Si substrate. A platinum (Pt) gate electrode is then deposited via RF magnetron sputtering, followed by the deposition of a HfO_x dielectric layer. The IGZO channel layer is subsequently deposited using sputtering techniques. Finally, aluminum (Al) source and drain electrodes are deposited via e-beam evaporation using a shadow mask, defining a channel with a length and width of 80 µm.

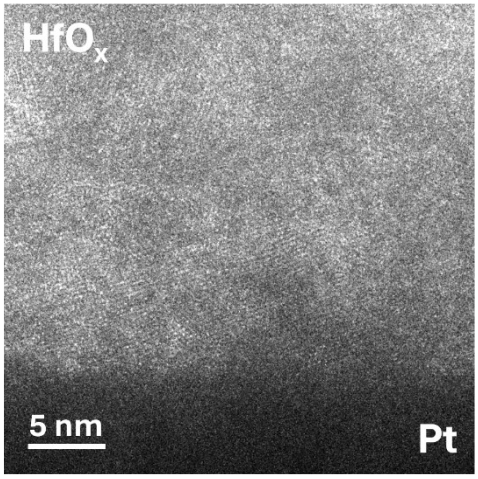

Figure S3. Cross-sectional TEM image of the IGZO/HfO_x/Pt structure, including a high-resolution TEM image highlighting the HfO_x/Pt interface.

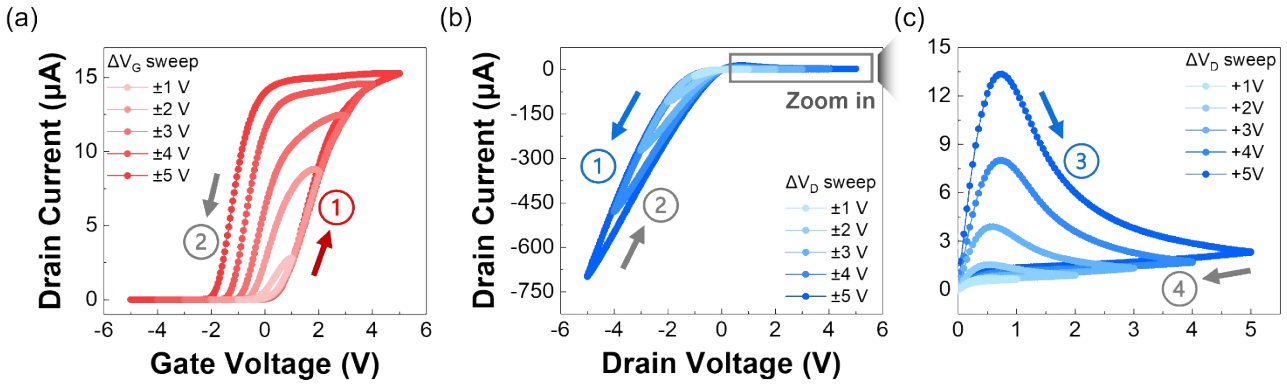

Figure S4. (a) Transfer curves measured over varying gate voltage sweep ranges (ΔV_G from ±1 V to ±5 V) at V_D = 100 mV. (b) Output curves measured over varying drain voltage sweep ranges (ΔV_D from ±1 V to ±5 V) at V_G = 100 mV. The progressive expansion of the hysteresis window with increasing sweep range highlights its influence on the current response and memory behavior. (c) The magnified plot of the positive V_D sweep in (b) highlights the observed clockwise hysteresis.

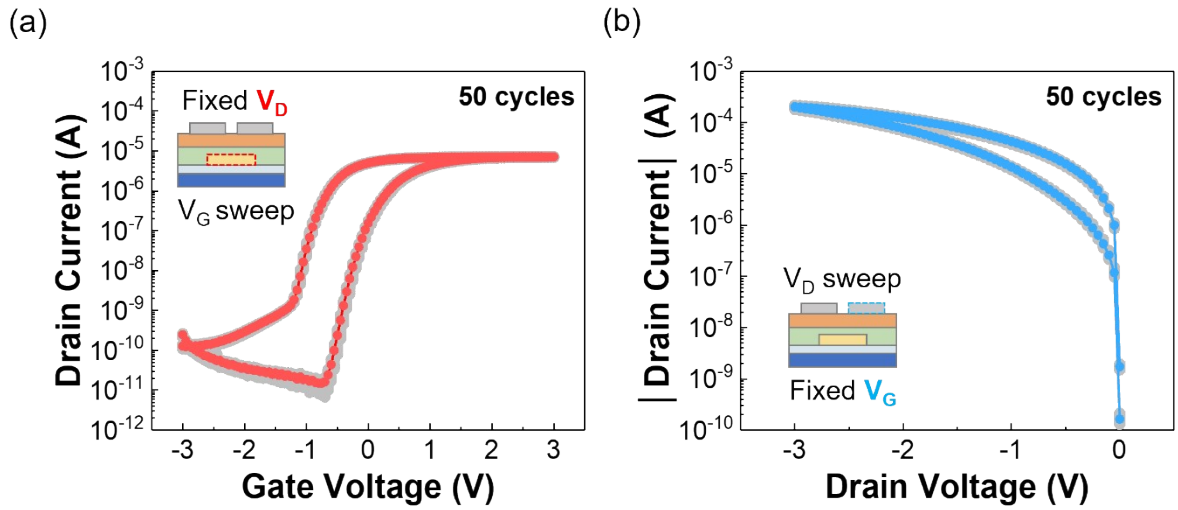

Figure S5. Consecutive (a) transfer curves at a constant V_D of 100 mV and (b) output curves at a constant V_G of 100 mV, obtained over 50 measurement cycles. The minimal variation in I-V curves across cycles highlights the stability and high repeatability of the device performance.

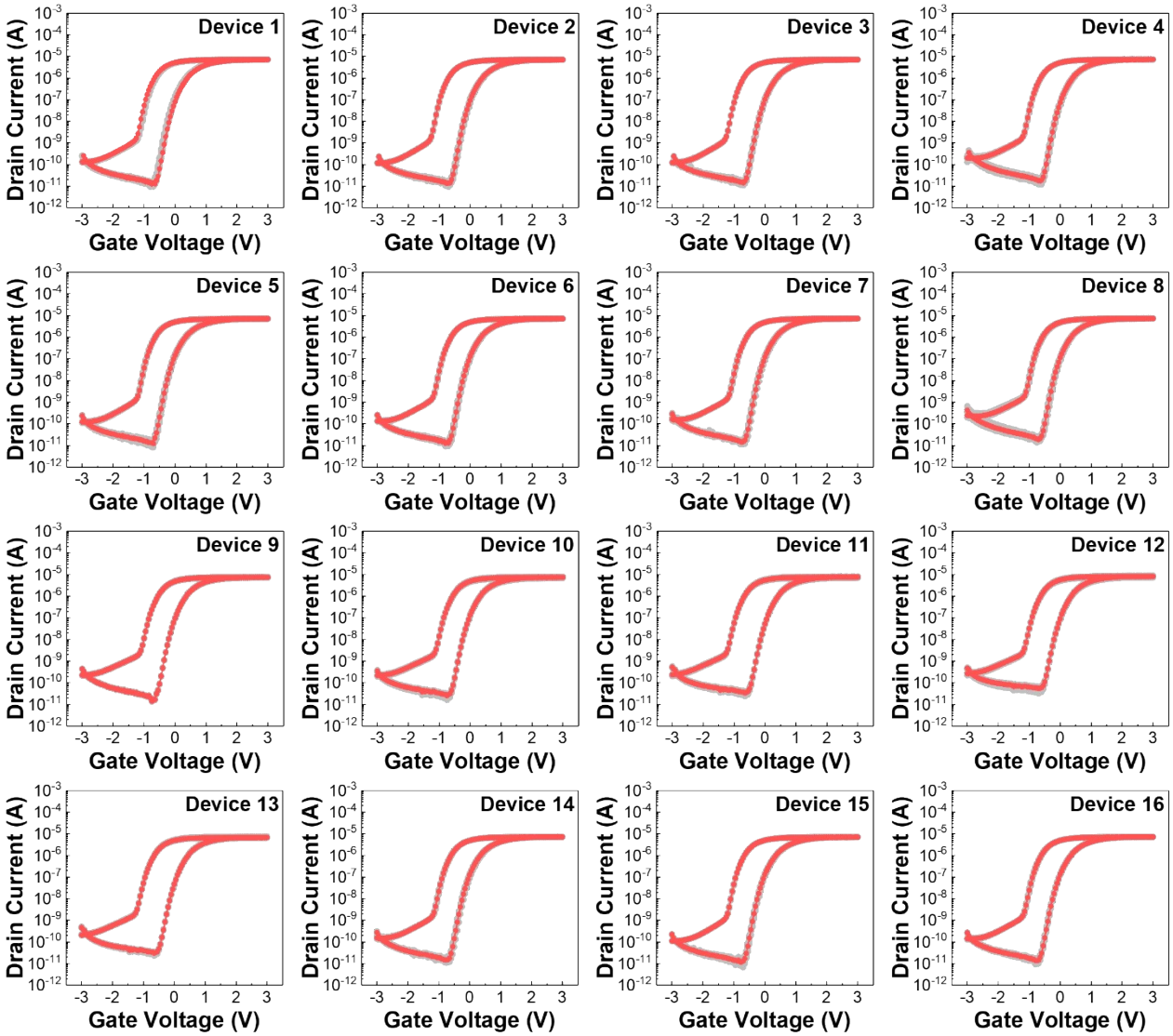

Figure S6. Device-to-device variation in transfer curves for sixteen devices at a constant V_D of 100mV. Each device was measured over 10 cycles.

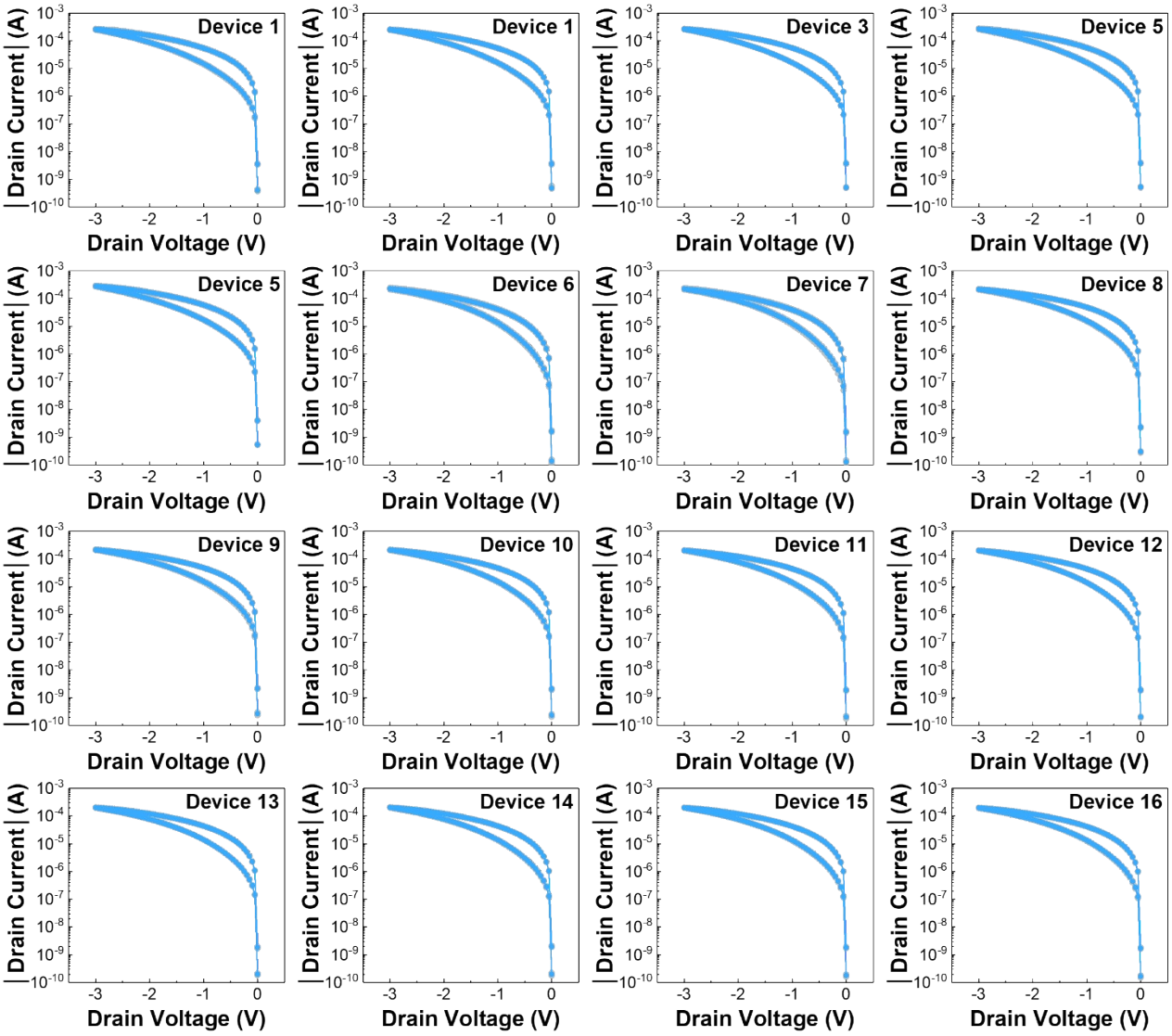

Figure S7. Device-to-device variation in output curves for sixteen devices at a constant V_G of 100mV. Each device was measured over 10 cycles.

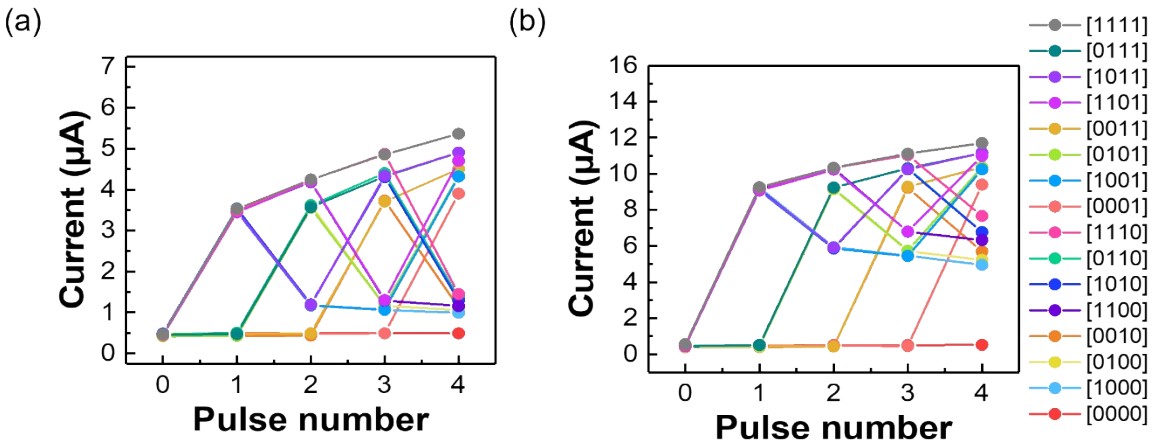

Figure S8. Current responses to 16 distinct 4-bit pulse sequences (0000 to 1111) measured at pulse heights of (a) 2.5 V and (b) 5.0 V, with a fixed pulse interval of 10 ms.

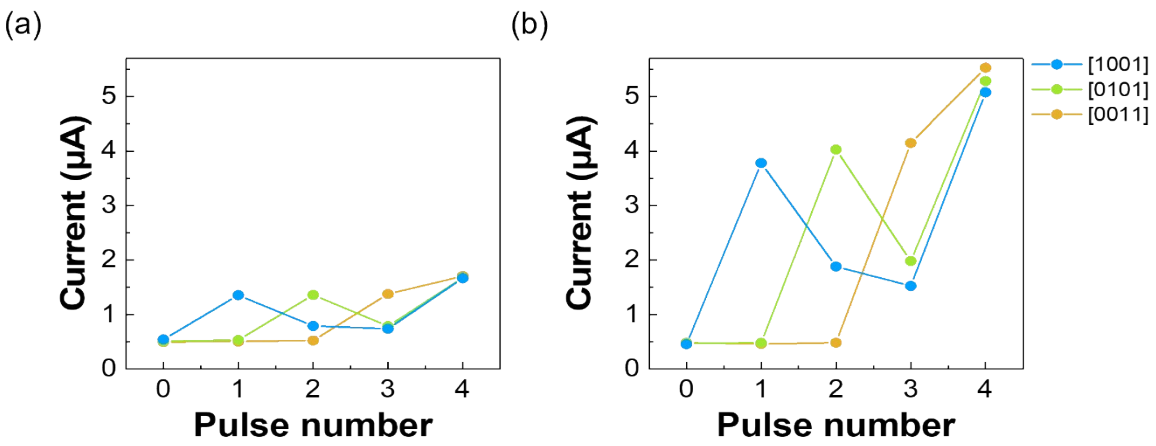

Figure S9. Analysis of current response and state differentiation under different pulse application conditions using three 4-bit pulse sequences (“0011,” “0101,” and “1001”). (a) Pulses applied only to the gate terminal. (b) Pulses applied simultaneously to drain and gate terminals.

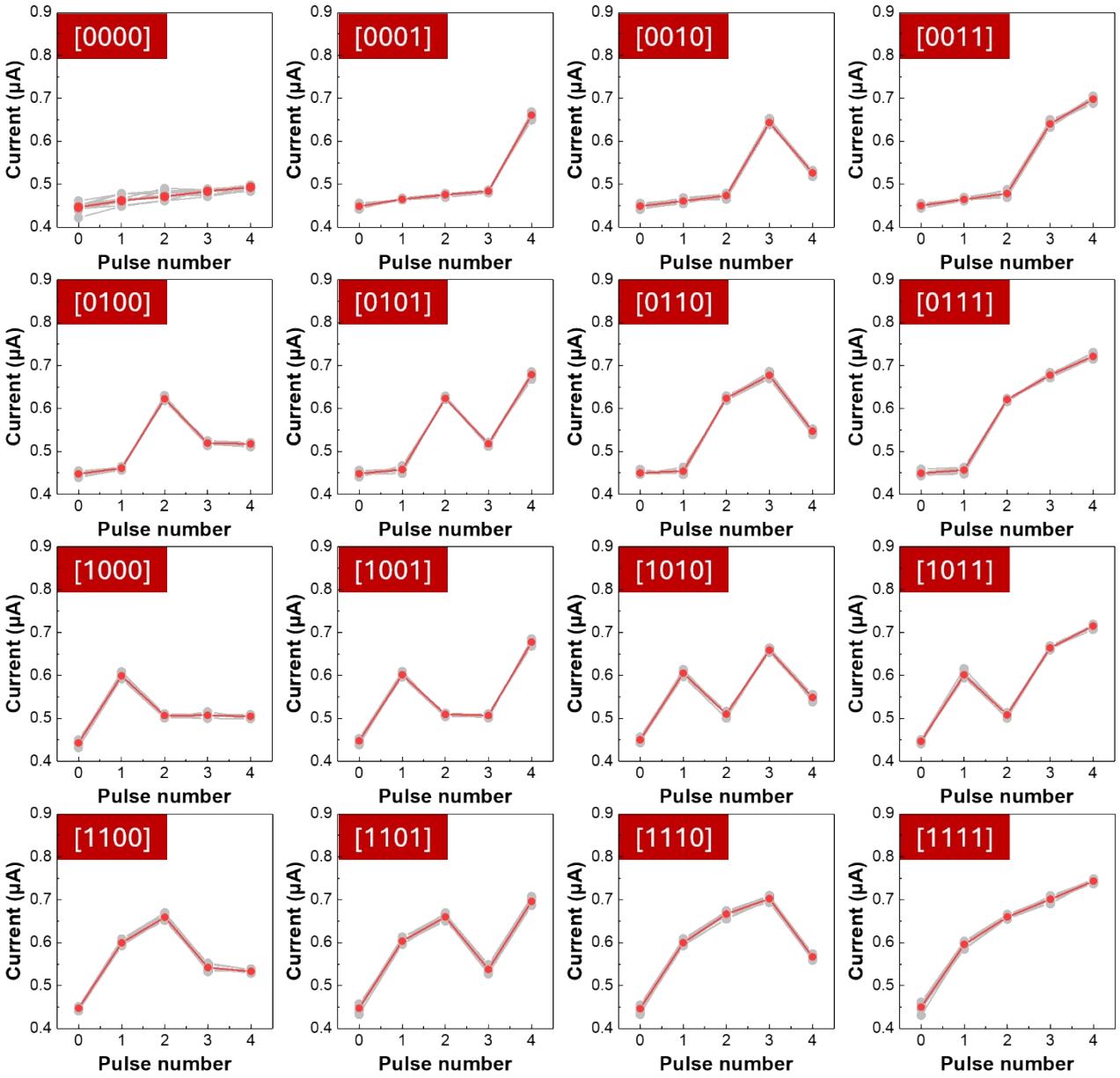

Figure S10. Cycle-to-cycle measurements of sixteen distinct states are generated by 4-bit pulse streams ranging from "0000" to "1111," with a pulse height of 0.5 V and a 1 ms interval. Each state was measured over 10 cycles, with variations in final conductance observed as 1.24% for "1100," 1.29% for "1010," and 0.95% for "1001".

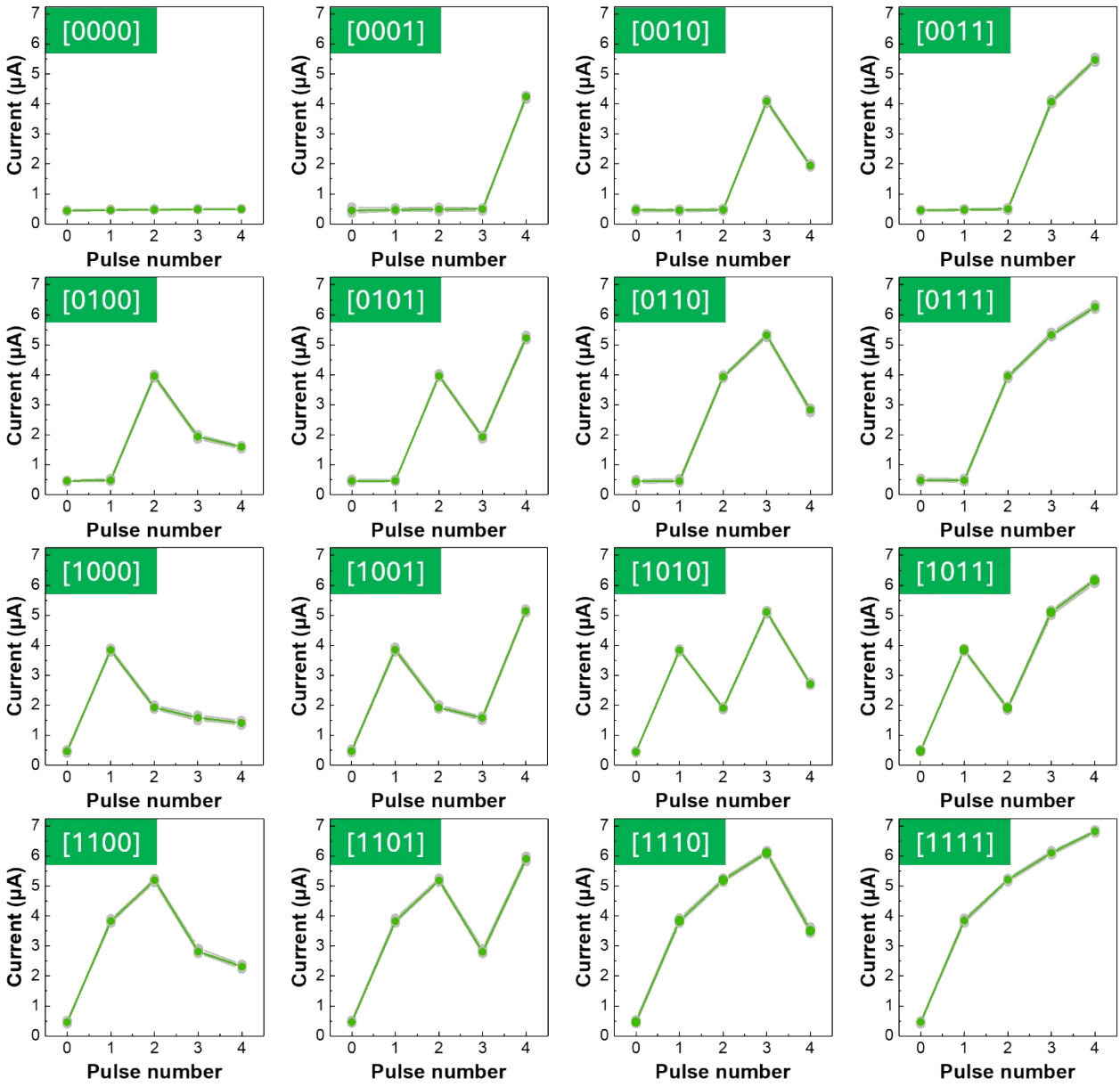

Figure S11. Cycle-to-cycle measurements of sixteen distinct states are generated by 4-bit pulse streams ranging from "0000" to "1111," with a pulse height of 2.5 V and a 1 ms interval. Each state was measured over 10 cycles, with variations in final conductance observed as 2.17% for “1100,” 1.23% for “1010,” and 0.89% for “1001."

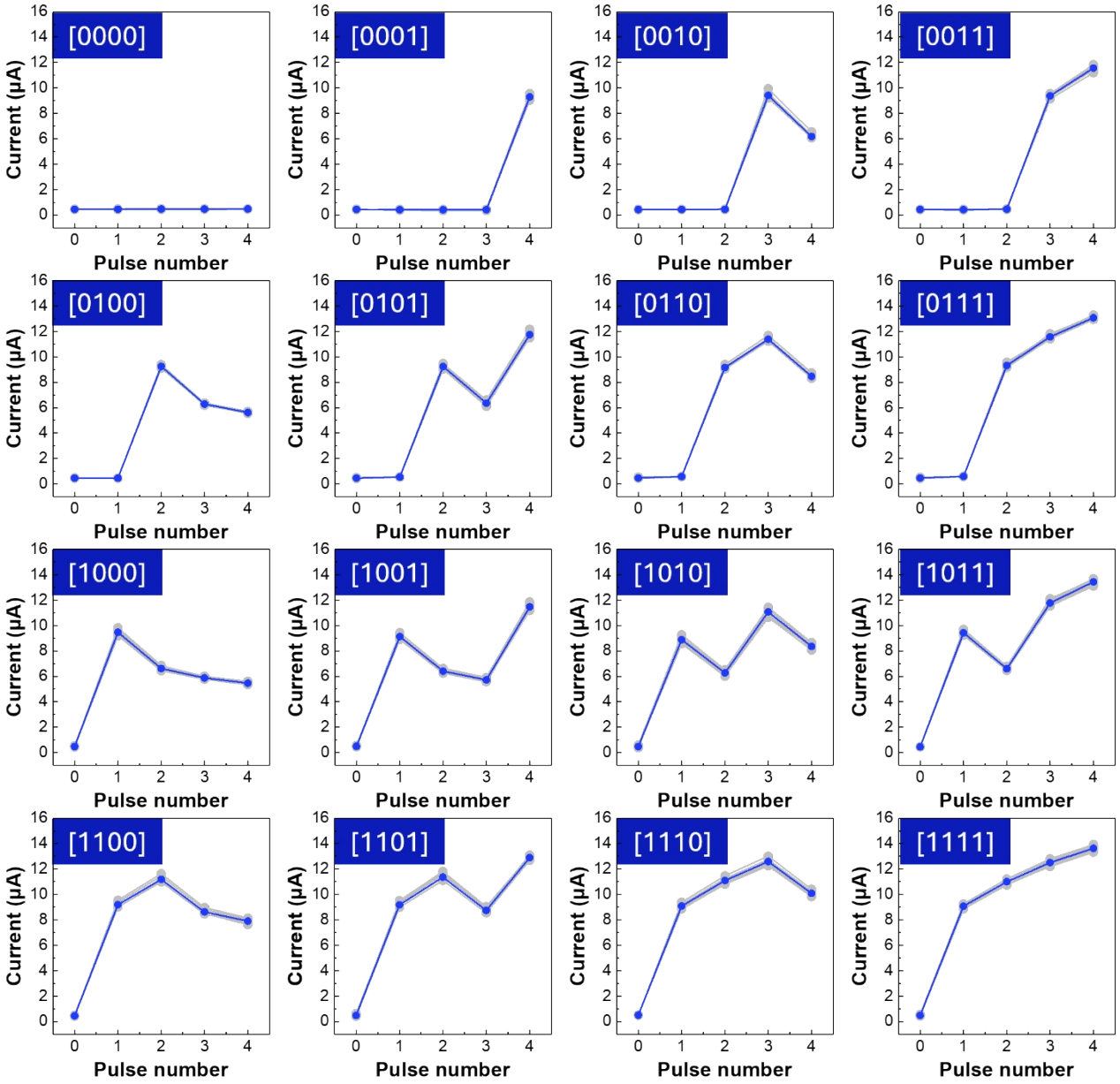

Figure S12. Cycle-to-cycle measurements of sixteen distinct states are generated by 4-bit pulse streams ranging from "0000" to "1111," with a pulse height of 5.0 V and a 1 ms interval. Each state was measured over 10 cycles, with final conductance variations observed as 1.87% for "1100," 2.03% for "1010," and 1.90% for "1001".

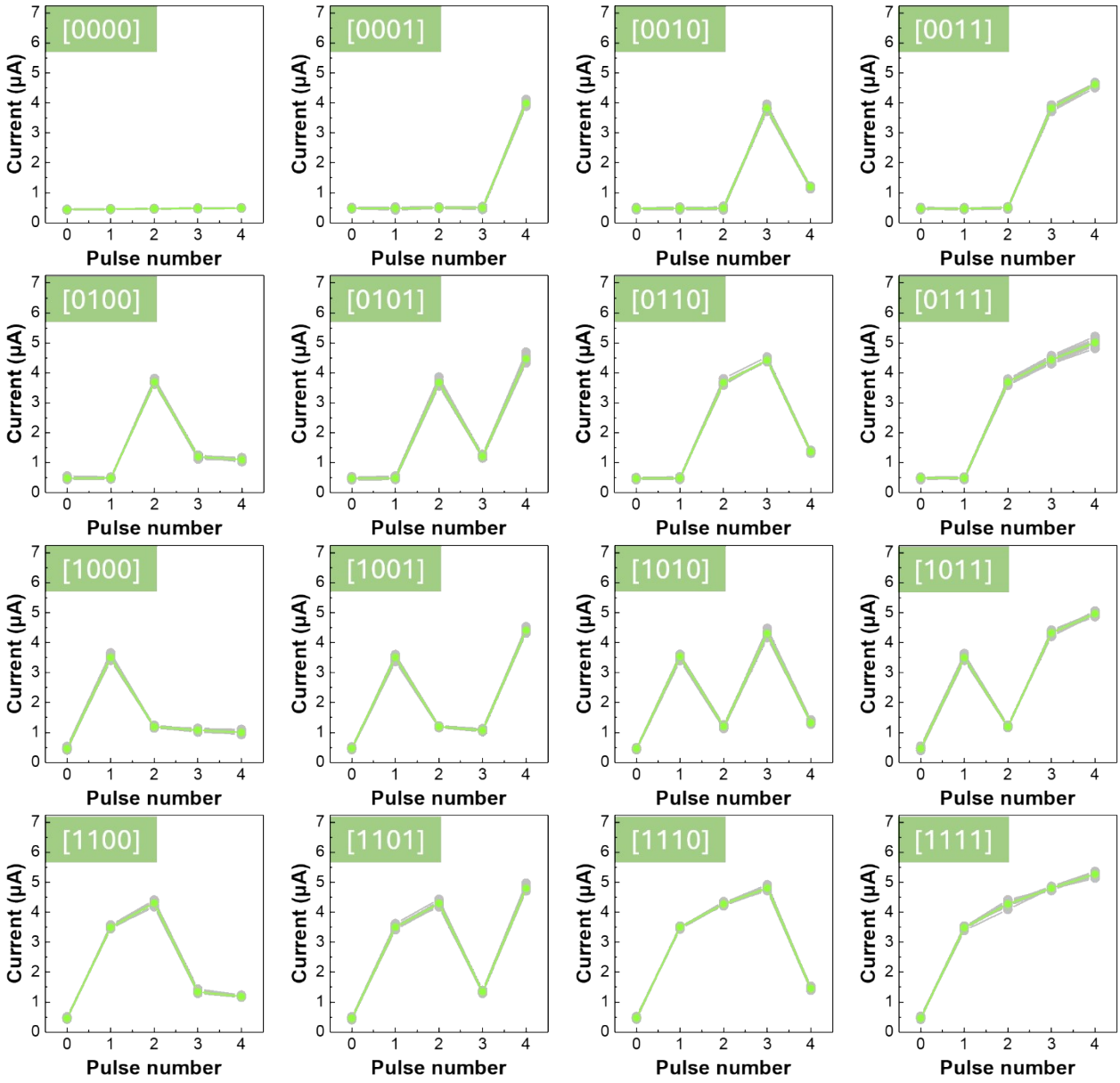

Figure S13. Cycle-to-cycle measurements of sixteen distinct states are generated by 4-bit pulse streams ranging from "0000" to "1111," with a pulse height of 2.5 V and a 10 ms interval. Each state was measured over 10 cycles, with variations in final conductance observed as 1.95% for "1100," 3.61% for "1010," and 1.82% for "1001".

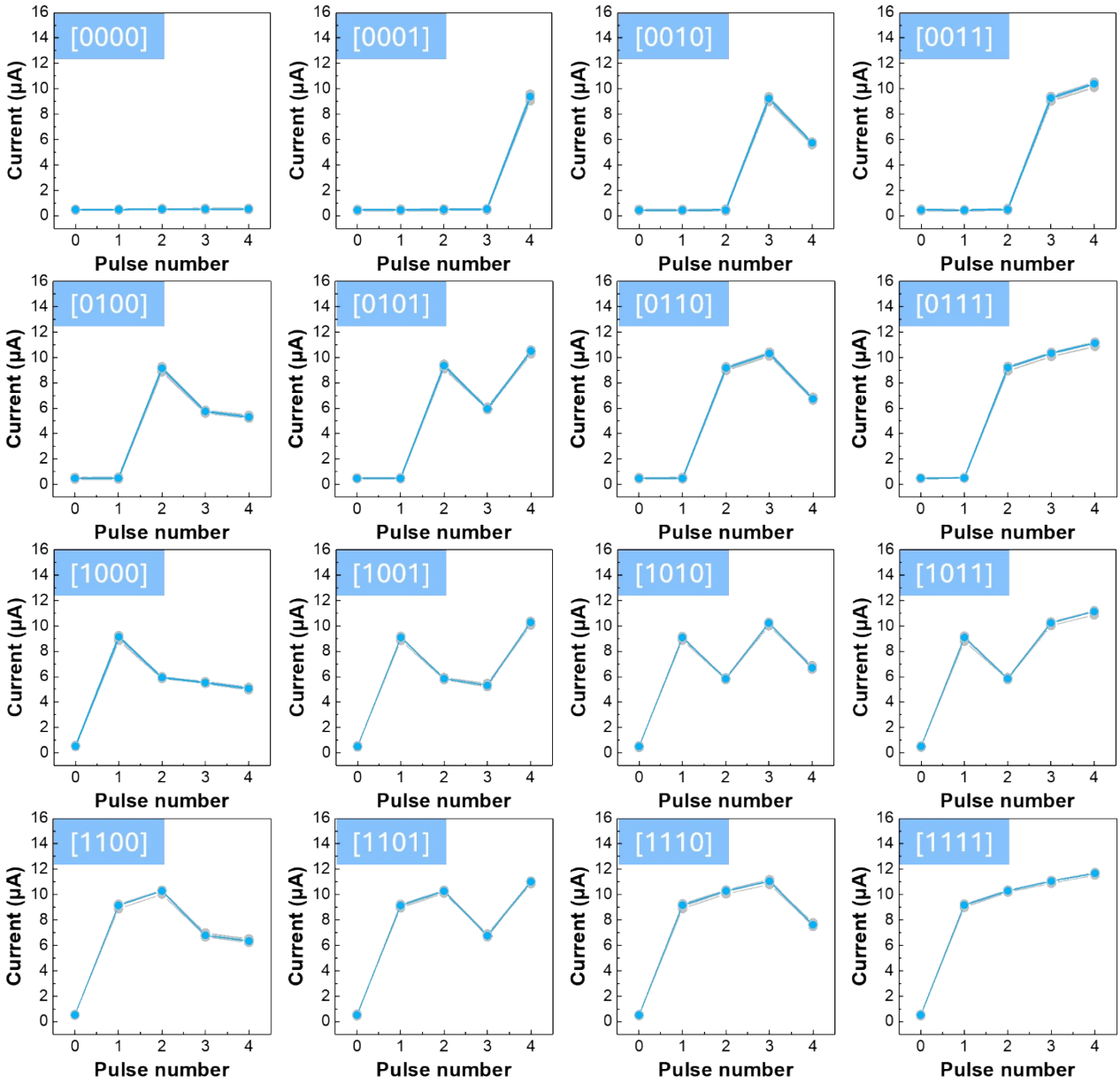

Figure S14. Cycle-to-cycle measurements of sixteen distinct states are generated by 4-bit pulse streams ranging from "0000" to "1111," with a pulse height of 5.0 V and a 10 ms interval. Each state was measured over 10 cycles, with variations in final conductance observed as 1.81% for "1100," 1.39% for "1010," and 0.84% for "1001".

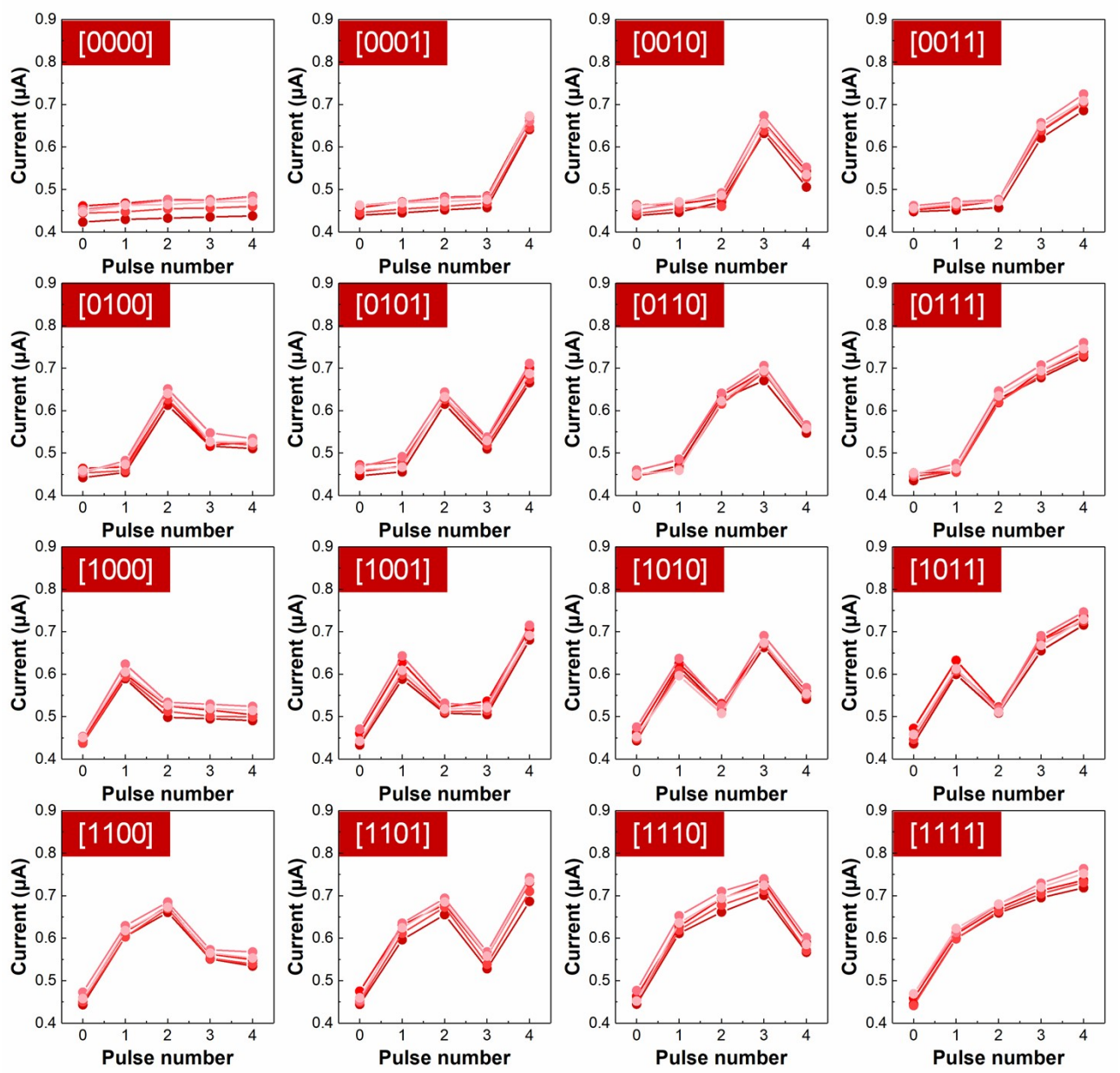

Figure S15. Device-to-device measurements of sixteen distinct states are generated by 4-bit pulse streams ranging from "0000" to "1111," with a pulse height of 0.5 V and a 1 ms interval. Each state was measured across five devices, with variations in final conductance observed as 2.36% for "1100," 1.81% for "1010," and 1.97% for "1001."

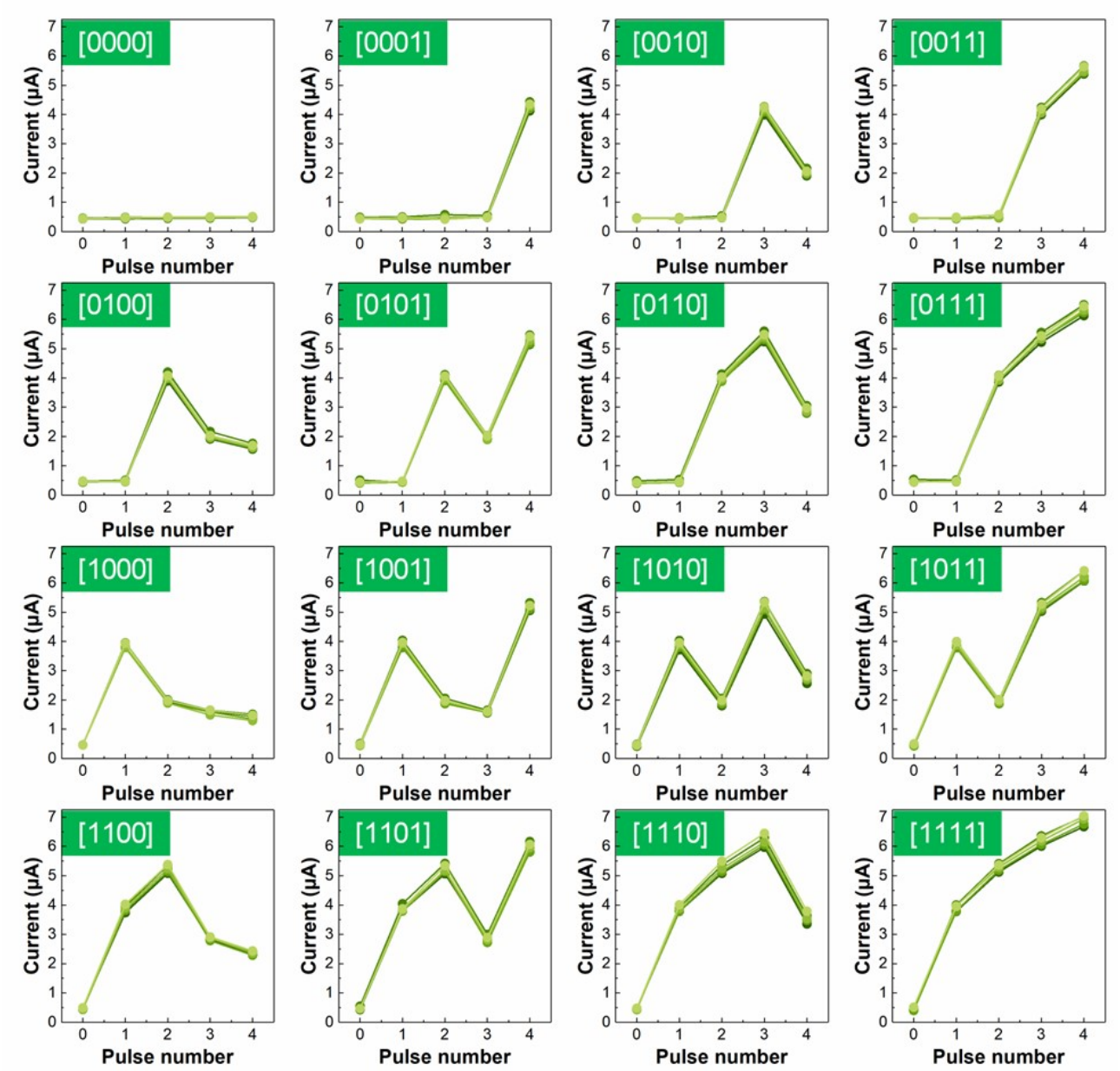

Figure S16. Device-to-device measurements of sixteen distinct states are generated by 4-bit pulse streams ranging from "0000" to "1111," with a pulse height of 2.5 V and a 1 ms interval. Each state was measured across five devices, with variations in final conductance observed as 2.68% for "1100," 4.71% for "1010," and 2.03% for "1001."

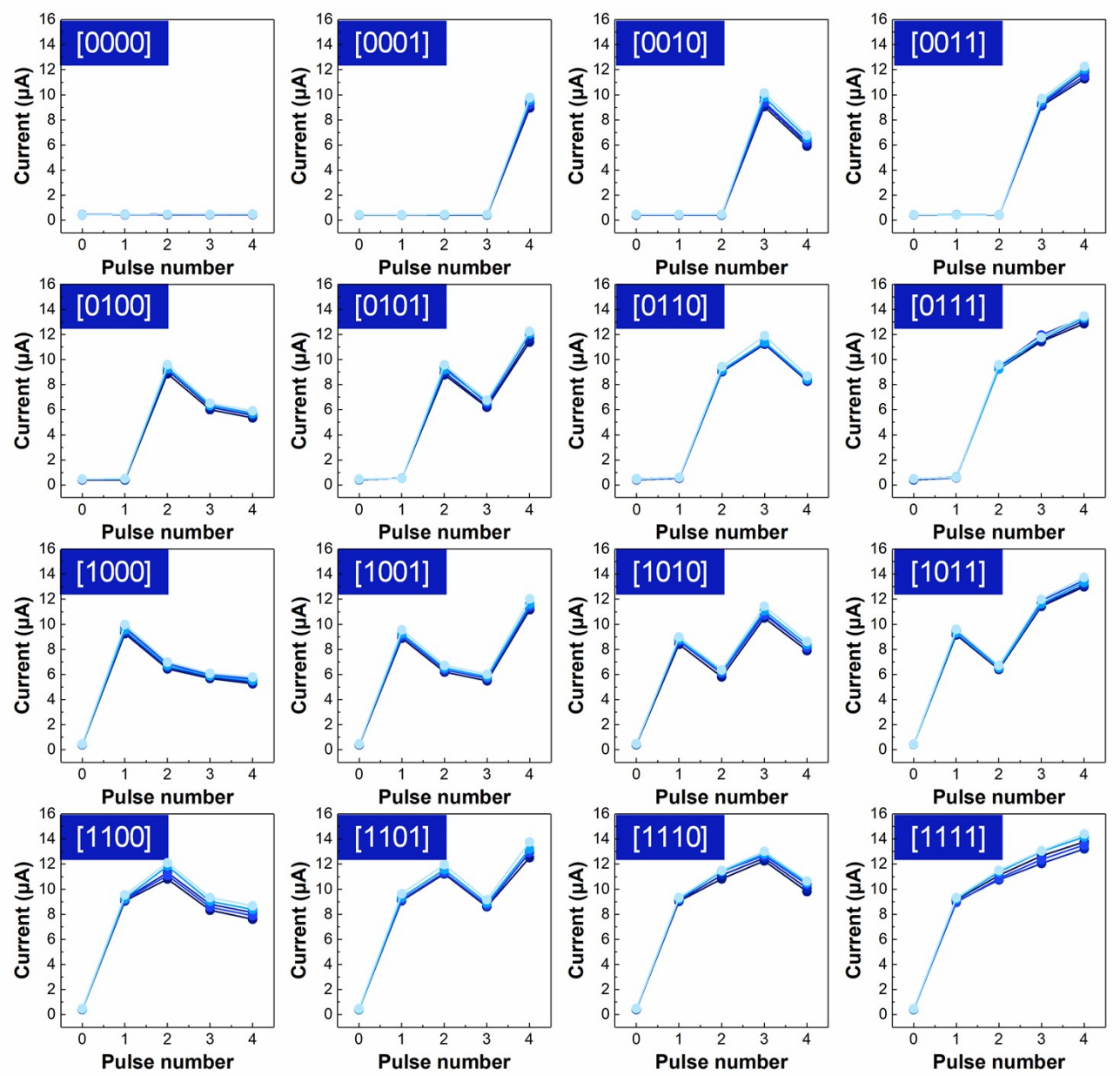

Figure S17. Device-to-device measurements of sixteen distinct states are generated by 4-bit pulse streams ranging from "0000" to "1111," with a pulse height of 5.0 V and a 1 ms interval. Each state was measured across five devices, with variations in final conductance observed as 5.11% for "1100," 3.37% for "1010," and 2.81% for "1001."

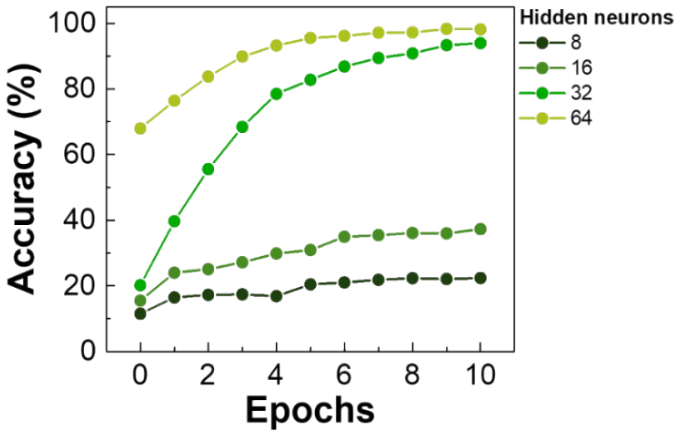

Figure S18. Impact of hidden layer size on model performance. The recognition accuracy was evaluated for models with hidden layer sizes of 8, 16, 32, and 64 neurons. Models with 8 and 16 neurons exhibited limited feature extraction, achieving only 22.4% and 37.3% accuracy after 10 training epochs. Increasing the size to 64 improved accuracies but introduced a risk of overfitting, as indicated by an initial accuracy of 67.9% at epoch 0. The optimal configuration of 32 neurons balanced feature extraction and overfitting mitigation, making it the most suitable choice.

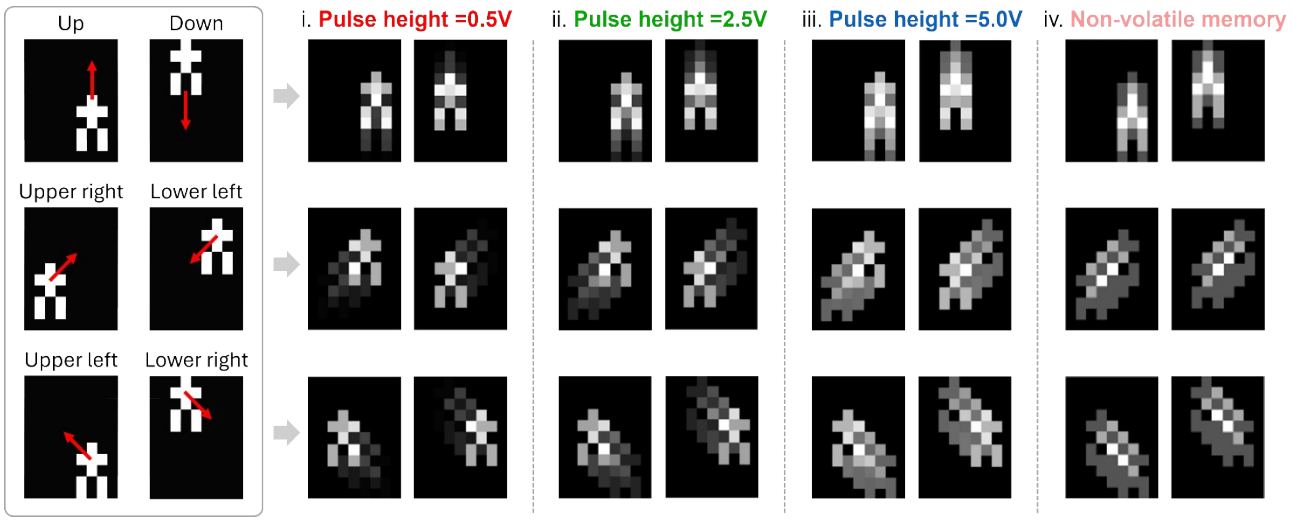

Figure S19. The feature-extracted images for various motion classes include up, down, upper-right, upper-left, lower-right, and lower-left under pulse heights of (i) 0.5 V, (ii) 2.5 V, (iii) 5.0 V, and (iv) non-volatile memory (NVM) conditions. These results demonstrate the clarity and accuracy of directional trajectories under different memory dynamics.

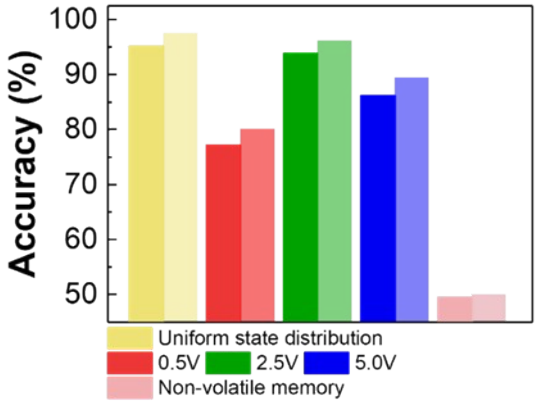

Figure S20. Impact of Gaussian noise on classification accuracy. This figure compares the classification accuracy under conditions with and without Gaussian noise. Conditions with noise are represented in darker shades, while those without noise are shown in lighter shades. With Gaussian noise included, the recognition accuracy is 93.9% at a pulse height of 2.5 V. In contrast, without Gaussian noise, the accuracy increases to 96.2%; however, this does not properly reflect device inhomogeneity in practical applications.

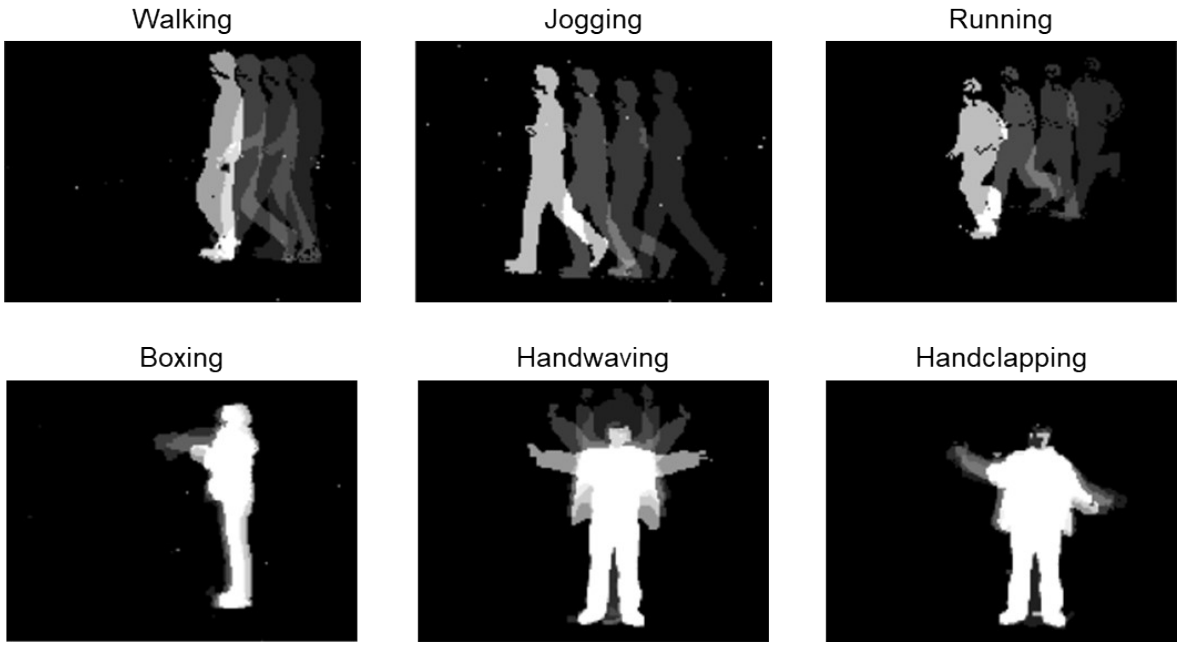

Figure S21. Feature-extracted images obtained by processing KTH dataset sequences with IGZO TFTs at a pulse height of 2.5 V. The device converts 4-bit time-series sequences into 16 distinct conductance states, effectively encoding motion trajectories.

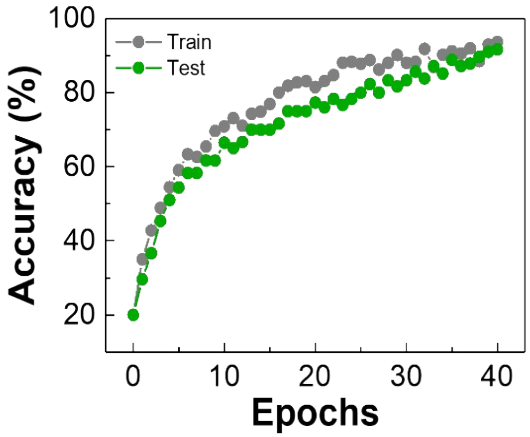

Figure S22. Classification performance of a neural network trained on feature-extracted images from the KTH dataset. Accuracy improves over training iterations, reaching 91.5%. Gray and green markers indicate training and testing accuracy, respectively.

Table S1. Cycle-to-cycle variability is assessed using sixteen distinct states, generated by pulse sequences ranging from "0000" to "1111," with pulse heights of 0.5 V, 2.5 V, and 5.0 V, measured over 10 cycles.

	Pulse height=0.5 V		Pulse height=2.5 V		Pulse height=5.0 V	
Pulse Sequence	Mean value (μ)	Variation	Mean value (μ)	Variation	Mean value (μ)	Variation
[0000]	4.92E-07	1.08%	5.03E-07	2.33%	4.80E-07	3.72%
[0001]	6.59E-07	1.43%	4.24E-06	1.02%	9.29E-06	1.86%
[0010]	5.28E-07	1.37%	1.95E-06	2.24%	6.18E-06	2.46%
[0011]	6.98E-07	0.94%	5.47E-06	1.02%	1.15E-05	1.99%
[0100]	5.20E-07	1.21%	1.59E-06	2.76%	5.62E-06	1.12%
[0101]	6.79E-07	0.78%	5.23E-06	0.89%	1.18E-05	2.41%
[0110]	5.47E-07	0.86%	2.83E-06	1.80%	8.47E-06	1.56%
[0111]	7.22E-07	1.06%	6.26E-06	0.79%	1.31E-05	1.11%
[1000]	5.12E-07	2.04%	1.41E-06	3.50%	5.47E-06	1.77%
[1001]	6.78E-07	0.95%	5.14E-06	0.89%	1.15E-05	1.90%
[1010]	5.47E-07	1.29%	2.70E-06	1.23%	8.36E-06	2.03%
[1011]	7.18E-07	0.98%	6.17E-06	0.93%	1.34E-05	1.42%
[1100]	5.34E-07	1.24%	2.31E-06	2.17%	7.91E-06	1.87%
[1101]	6.97E-07	1.39%	5.90E-06	0.96%	1.29E-05	1.12%
[1110]	5.67E-07	1.38%	3.51E-06	1.73%	1.01E-05	1.75%
[1111]	7.39E-07	1.01%	6.83E-06	0.52%	1.36E-05	1.65%

Table S2. Device-to-device variability is evaluated using sixteen distinct states, generated by pulse sequences ranging from "0000" to "1111," with pulse heights of 0.5 V, 2.5 V, and 5.0 V, measured across five different devices.

	Pulse height=0.5 V		Pulse height=2.5 V		Pulse height=5.0 V	
Pulse Sequence	Mean value (μ)	Variation	Mean value (μ)	Variation	Mean value (μ)	Variation
[0000]	4.96E-07	3.50%	5.01E-07	2.65%	4.81E-07	3.91%
[0001]	6.58E-07	2.22%	4.28E-06	2.83%	9.38E-06	3.38%
[0010]	5.33E-07	3.31%	2.02E-06	4.80%	6.32E-06	5.47%
[0011]	7.05E-07	1.97%	5.52E-06	2.24%	1.18E-05	3.37%
[0100]	5.23E-07	1.68%	1.66E-06	4.68%	5.65E-06	3.75%
[0101]	5.26E-07	2.19%	5.30E-06	2.67%	1.19E-05	2.92%
[0110]	5.58E-07	1.28%	2.91E-06	3.71%	8.45E-06	1.79%
[0111]	7.41E-07	1.78%	6.33E-06	2.42%	1.32E-05	1.81%
[1000]	5.07E-07	2.57%	1.42E-06	6.34%	5.52E-06	3.80%
[1001]	6.97E-07	1.97%	5.19E-06	2.03%	1.15E-05	2.81%
[1010]	5.54E-07	1.81%	2.74E-06	4.71%	8.24E-06	3.37%
[1011]	7.31E-07	1.59%	6.24E-06	2.74%	1.33E-05	2.25%
[1100]	5.49E-07	2.36%	2.36E-06	2.68%	8.14E-06	5.11%
[1101]	7.21E-07	3.12%	5.97E-06	2.58%	1.31E-05	3.51%
[1110]	5.83E-07	2.43%	3.56E-06	4.57%	1.03E-05	3.30%
[1111]	7.40E-07	2.39%	6.89E-06	2.38%	1.38E-05	3.44%